Regularization in Maximum Log-likelihood Method for CRISM Hyperspectral Image Cube. L. He[1], R. E. Arvidson[2], J. A. O'Sullivan[1], and D. V. Politte[1], [1]Department of Electrical and Systems Engineering, Washington University in St. Louis, [2]Department of Earth and Planetary Sciences, Washington University in St. Louis.

Introduction: The Compact Reconnaissance Imaging Spectrometer for Mars (CRISM) on the Mars Reconnaissance Orbiter (MRO) is a push-broom hyperspectral imaging spectrometer from 362 to 3920 nm with 6.5 nm spectral band spacing and the smallest ground pixel size of 18 m. Since 2010, images have also been acquired using a gimbal led, along track oversampled (ATO) model, with significant pixel overlapping in the along-track direction. The overlap allows reconstruction of map-projected images with 9 to 12 m/pixel, depending on the degree of overlap. For reference CRISM operates as S (362 to 1030 nm) and L (1036 to 2650 nm) imaging spectrometers. In this abstract we describe key improvements of our original log maximum likelihood method (MLM) for regularization of CRISM data [1].

Initial Processing: Two processing steps are necessary before application of the MLM procedures: 1. Retrieval of Single Scattering Albedos (SSAs) and 2. Extrema removal using a median filter. SSA is the ratio of scattering efficiency to scattering plus absorption efficiencies of a single particle. The spectral radiances from CRISM are first converted to I/F by dividing by the solar spectral radiance at Mars at the time of the observation. Discrete Ordinates Radiative Transfer (DISORT)-based processing and the Hapke function for surface scattering are used to retrieve SSA from I/F data [1]. A median filter (bit error filter) designed by Eliason and McEwen [2] is utilized to remove extreme noise spikes in the L data because of degraded cooler operation, and introduction of time and space variable responses within the 2D detector plane [3]. The results of the preprocessing steps are S and L sensor space data cubes in SSA units.

Maximum Log-likelihood Method: Data are acquired in sensor space and the intent is to reconstruct the best cube projected onto the surface. The transfer function is a linear mapping from the surface to the sensor space. Estimates are the mapping results in the sensor space after applying the transfer function to the images on the surface. The reconstruction problem comprises minimizing the discrepancy between the measurements and their estimates. We have shown that the SSA data after median filtering are well modeled as being Poisson distributed [1] with the estimates as the mean values of the distribution. Minimizing the I-divergence between measurements and estimates is equivalent to maximizing the log-likelihood, and thus we use I-divergence as our discrepancy measure. The Maximum Log-likelihood Method (MLM) derived in [1] solves this optimization problem.

Regularization: The ATO data are non-uniformly sampled, so the forward operator from the surface to the sensor space is ill-conditioned, making the reconstruction problem ill-posed. In order to enhance stabilities in the reconstructed image estimates, we introduce spatial penalty and spectral penalty functions

$$\begin{cases} \Phi_1(x) = \sum_{x_i} \beta_i \sum_{x_k \in NA(x_i)} \delta \ln \cosh\left[\frac{x_i - x_k}{\delta}\right] \\ \Phi_2(x) = \sum_{x_i} \eta_i \sum_{x_j \in NE(x_i)} \left(-\ln \frac{x_i}{x_j} - 1 + \frac{x_i}{x_j}\right) \end{cases}$$

where x_i is one pixel in the image space and $NA(x_i)$ and $NE(x_i)$ are spatial and spectral neighborhood of x_i. Fig. 1 shows the penalized MLM algorithm.

Algorithm Maximum Log-likelihood Method with Regularization

Input: measure data $d = [d_1, \cdots, d_N]^T \in \mathbb{R}_+^N$, transfer function $H \in \mathbb{R}^{N \times M}$, maximum iterations $maxiter$, penalty parameter β_i, δ, η_i
Output: reconstructed image $c = [c_1, \cdots, c_M]^T \in \mathbb{R}_+^M$, estimate data $a = [a_1, \cdots, a_N]^T \in \mathbb{R}_+^N$
Start:
Initialize $c^{(1)}$ and compute sensitivity $h = H^T ones \in \mathbb{R}^N$ where $ones = [1, \cdots, 1]^T \in \mathbb{R}^M$
for $t = 1 \rightarrow maxiter$
Forward Projection: $a^{(t)} = Hc^{(t)}$
Data Modification: $b_i^{(t)} = d_i / a_i$
Backward Projection: $f = H^T b$
Update: $c^{(t+1)} = \arg \min_{c=[c_1 \cdots c_M]} \Sigma_i - c_i^{(t)} f_i^{(t)} \ln c_i + h_i c_i + \Phi_1(c) + \Phi_2(c)$
end
Note:
1. H^T is the transpose of H; 2. N is the number of measure data and M is the number of image pixels;
3.Update step is solved by our fast algorithm.

Fig. 1 MLM algorithm.

Our previous approach for incorporating the penalty functions used constant weights $\beta_i = \beta$ and $\eta_i = \eta$ for all pixels and bands. This approach produced artifacts in the resulting images and spectra. Row artifacts were produced spatially because the penalty term was weighted higher than the I-divergence in undersampled areas, resulting in over-smoothing. In addition, lack of consideration of variations in the noise level for different wavelengths led to regularized spectra with unacceptably high levels of residual noise. Therefore, we derived weights that depend on spatial sampling intervals and the spectral noise level as a function of wavelength.

Spatial weights. Given the spatial transfer function, we compute the total contribution of each pixel in the projected image space to all data in the sensor space. This is the sensitivity function. Values in the sensitivity function range over 20 orders of magnitude due to along-track oversampling variations. In other words, some areas are highly oversampled whereas others are highly undersampled. Making the weights in the spatial penalty proportional to the sensitivity values equalizes the relative importance of the I-divergence and penalty

terms, and eliminates the row artifacts associated with high degrees of undersampling.

Spectral weights. The spectral noise level as a function of wavelength for the entire scene is quantified using high frequency information as exemplified by its spectrogram (Fig. 2). The high frequency information is scaled by a monotonically increasing concave function to compute the spectral weights η_i, i.e., the magnitude of the spectral penalty then depends on the noise level, with higher penalties associated with noisier wavelengths.

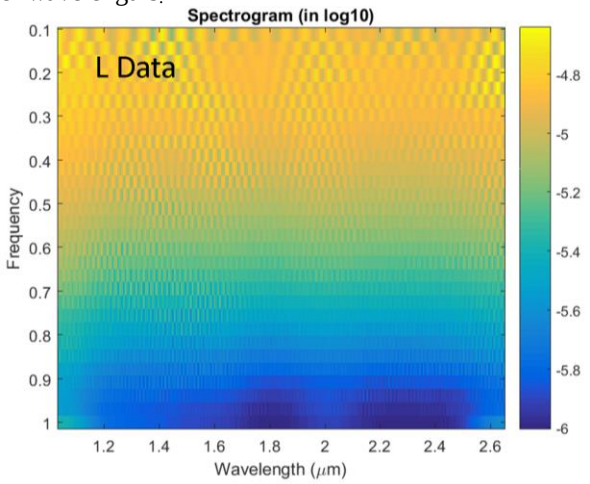

Fig. 2 Mean spectrogram of scene ATO0002DDF9 is shown with color-coded relative noise levels. The vertical axis is the spectral Fourier frequency. Low noise levels at high frequency are found between ~1.7 to 1.9 and 2.1 to 2.5 μm, consistent with the performance of the CRISM instrument.

Performance Analysis: Three ATOs covering the traverses taken and planned for the Opportunity rover were used to test performance of the new MLM procedures. ATO0002DDF9 is illustrative of results, with the original data processed to SSA values only (Fig. 3a) compared to values run through the median filter and updated MLM procedures (Fig. 3b). Example results are provided in Figs. 4 and 5.

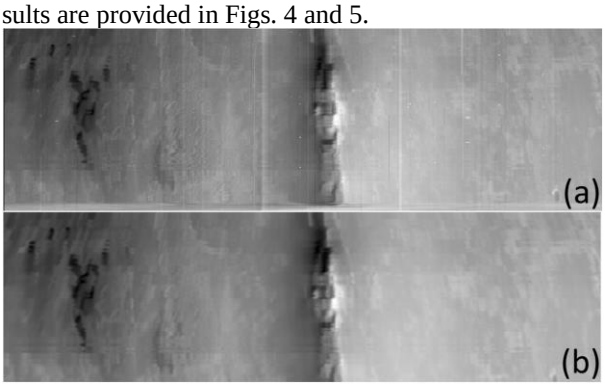

Fig. 3 Comparison between pre-processing and post-processing. (a) shows sensor space SSA data before median filter and MLM applications whereas (b) shows the output from our procedures. Data are shown for the band at 1.7038 μm. Note the removal of random spikes and column dependent noise.

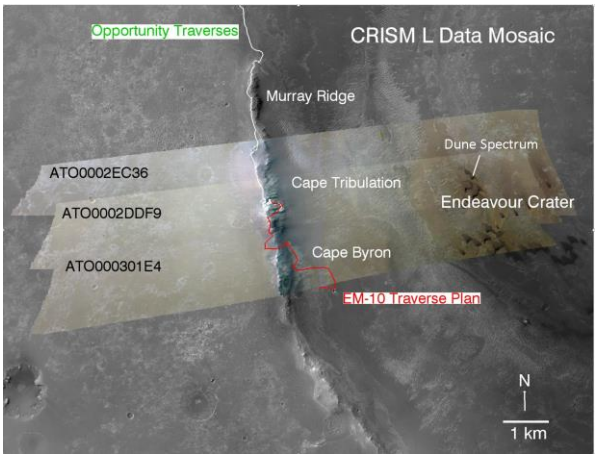

Fig. 4 Three test scenes projected onto a HiRISE base map are shown, along with Opportunity traverses. Spectrum for dune shown in Fig. 5.

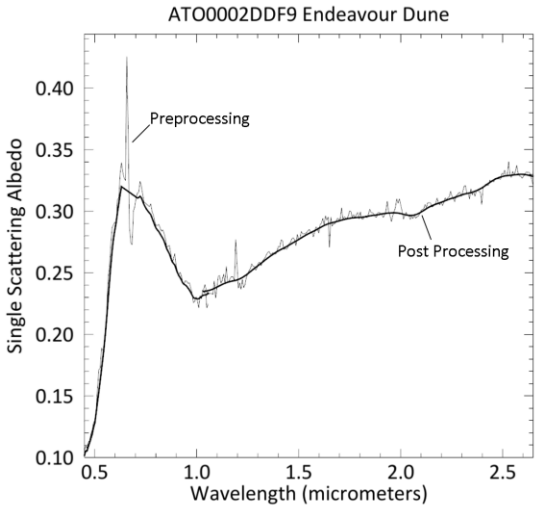

Fig. 5 Twenty-five pixels mean spectra are plotted for the dune (Fig. 4) for the S and L projected data. Thin lines represent SSA data before median filter and MLM processing and thick lines show final results. The regularized spectra closely follow the original data without noise excursions and are indicative of spectral dominance by ferrous silicates, except at short wavelengths, where a fine-grained ferric oxide signature is evident.

References: [1] Kreisch C. D. et al. (2017) *Icarus* 282, 136-151. [2] Eliason E. M. and McEwen A. S. (1990) *Photogramm. Eng. Remote Sens.*, 56.4, 453-458. [3] Murchie S. et al. (2007) *J. Geophys. Res.: Planets*, 112.E5.